



# Fused granulate fabrication of injection molding inserts from high-performance ULTEM 9085™ thermoplastic for cosmetic packaging industry

Albert Curmi<sup>1</sup> · Arif Rochman<sup>1</sup>

Received: 30 October 2023 / Accepted: 10 April 2024  
© The Author(s) 2024

## Abstract

RTIM refers to the integration of rapid tooling (RT) using additive manufacturing (AM) with injection molding (IM). Due to the use of raw material (pellet), screw extrusion, fused granulate fabrication (FGF) allows for a cost-effective and versatile production of RTIM inserts especially compared to other material extrusion (MEX) AM processes, such as fused filament fabrication (FFF). This study 3D printed RTIM inserts out of high-performance thermoplastic polyetherimide (PEI) (ULTEM 9085) in granular form, using an in-house developed FGF system. A cosmetic compact was used as a case study part with a simplified design. A dynamic mechanical analysis (DMA) conducted on FGF ULTEM 9085 demonstrated that the strength of the inserts is sustained up to 140 °C, which suits injection molding using polypropylene (PP). Optical profilometry of the FGF 3D printed RTIM inserts demonstrated that when using a 0.4 mm nozzle, the flat surfaces produced had microscopic gaps larger than 10<sup>-1</sup> mm. These gaps are sufficiently large so that melt of low viscosity polymer is able to flow through, which leads to undesired part flash. The IM experiments confirmed that the inserts were capable of producing PP parts but with the predicted flash. Simulated part deflection differed both on geometry and magnitude from the actual deflection measured by optical profilometry. A total of 36 prototype parts were produced before the inserts failed due to poor inter-layer bond strength. FGF RTIM using ULTEM 9085 is deemed suitable for prototype part production. Improving the inter-layer bond strength and decreasing part complexity could increase the number of parts produced.

**Keywords** Rapid tooling · Fused granulate fabrication · Injection molding · High performance · Material extrusion

## 1 Introduction

Additive manufacturing (AM) can be used for rapid prototyping (RP), rapid tooling (RT), and rapid manufacturing (RM) [1]. Fused granulate fabrication (FGF) is an AM technology which is based on material extrusion (MEX) and utilizes granules rather than filament as done in fused filament fabrication (FFF). The raw material versatility provided by FGF allows for a more cost-effective and discerning material choice. In the case of RT for injection molding (IM), often referred to as RTIM, high-performance polymers may be

used to produce bespoke mold inserts for prototype production or low-batch production of end products with typical injection molding quality. In contrast to RP using RT, direct RP using an AM technology even using the same desired grade of material will create prototypes with incongruent mechanical properties due to the disparate processing conditions [2, 3].

Vat polymerization AM techniques for RTIM have been studied by multiple research groups [4–10]. This group of technologies has a high level of surface finish control, capable of obtaining smooth or textured surfaces by design. Such surface quality is important for RTIM inserts but material properties also play a crucial role. Studies by Davoudinejad et al. and Moritz et al. showed that the higher the mold temperature, the lower the service life of the insert and the produced part quality [4–6]. MEX 3D printed inserts are not capable of reaching the same surface quality as vat polymerized inserts [11] but can achieve better mechanical performance. MEX systems are capable

✉ Arif Rochman  
arif.rochman@um.edu.mt

Albert Curmi  
albert.curmi.16@um.edu.mt

<sup>1</sup> Department of Industrial and Manufacturing Engineering,  
University of Malta, Msida 2080, Malta

of 3D printing using high performance thermoplastics such as polyether ether ketone (PEEK) and polyetherimide (PEI) which can have even better thermal resistance and strength than their resin counterparts for vat polymerization AM. PEEK filled with carbon fiber was used for FFF to produce mold inserts by Rodzeń et al. which showed encouraging results. The combination of high temperature resistance, strength, and toughness and the use of a simple insert with no features resulted in the reported production of 100 inserts by IM with no apparent damage to the insert [12]. Acrylonitrile butadiene styrene (ABS) [13, 14], polylactic acid (PLA) [15], and polyamide (PA) [13, 14, 16] have also been applied for RTIM with good success but with a lower performance and part quality compared to PEEK-CF inserts.

A common issue among all MEX research works is the large presence of flash on the molded parts. All polymeric RTIM inserts also suffer from a low thermal conductivity compared to metallic molds. Better cooling performance is often necessary and can be achieved by using conformal cooling channels [17], better heat conductivity [18] or longer cooling time [17, 19].

Apart from PEEK, PEI (e.g., ULTEM 9085) is another high-performance polymer with a wide usage in FFF 3D printing. ULTEM 9085 is PEI blended with polycarbonate (PC) [20], having a heat deflection temperature of 153 °C [21], which makes it applicable as an RTIM material. The only published study involving PEI AM for RTIM, was presented by Farioli et al. but using ULTEM 1010 and FFF 3D printing [22]. Similar to most studies carried out on RTIM, this study used a simple part geometry, resulting in a simple insert design and print. This simplification neglects the real-life complexity of common day objects, where RTIM process would be applied. Apart from empirically testing more complex applications of RTIM, simulation may also be viable route. The issue with such techniques is to ensure that the anisotropic properties and internal porosity, both micro and macro, are reflected in the simulation process. With regard to thermal behavior during IM, the discrepancies could be substantial. Additionally, the current published research lacks detailed thermal measurements which limits

understanding of the effects of low heat dissipation of polymeric RTIM inserts.

The aim of this study was to investigate PEI ULTEM 9085 for RTIM using an in-house built FGF 3D printing system. This novel application of ULTEM 9085 for RTIM could potentially extend the inserts lifespan while maintaining acceptable insert quality. This, coupled with the reduction in costs when using FGF for insert production, could enhance RTIM's cost-effectiveness and application in industry. A cosmetic packaging case study was used to showcase the challenges of complexity. The accuracy of the FGF process was evaluated for dimensional fidelity, by comparing the inserts to the original 3D CAD model. Additionally, the RTIM process was also investigated, particularly regarding thermal behavior including cooling rate and potential hot spots in the inserts. Dimensional accuracy and quality of the produced parts were also analyzed. Beyond empirical testing, the IM process was simulated to predict the expected part deflection and to verify the applicability of such a simulation to an RTIM process.

## 2 Materials and methods

### 2.1 Case studies

A cosmetic compact studied by Vella et al. [11] will be used as the case study part for this work as shown in Fig. 1. This case study originates from the cosmetic packaging industry which often requires multiple prototyping steps in its design cycle [23]. The original part was simplified to as shown in Fig. 2a, similarly done by Vella et al. [11].

Case study 1 had a complex geometry which can be challenging to 3D print using MEX additive manufacturing processes. Both injection and ejection side inserts had shallow curved surfaces as highlighted and magnified in Fig. 2a. It is relatively difficult to achieve a high quality of such shallow curved surfaces when using MEX systems especially if the inserts are printed horizontally i.e., flat on the build plate. Such shallow curves lead to a terraced face where the layer height used for the 3D printing process limits how well

**Fig. 1** Original cosmetic compound upon which the case studies were inspired

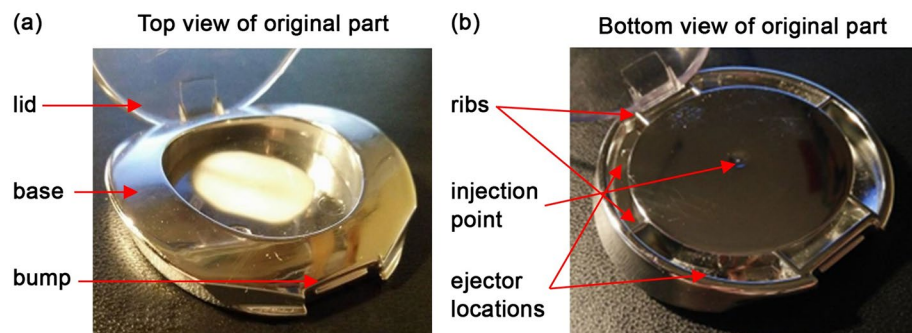


**Fig. 2** Case study 1 inserts and part (a) with detail of stepped surface (b) and weak features (c)

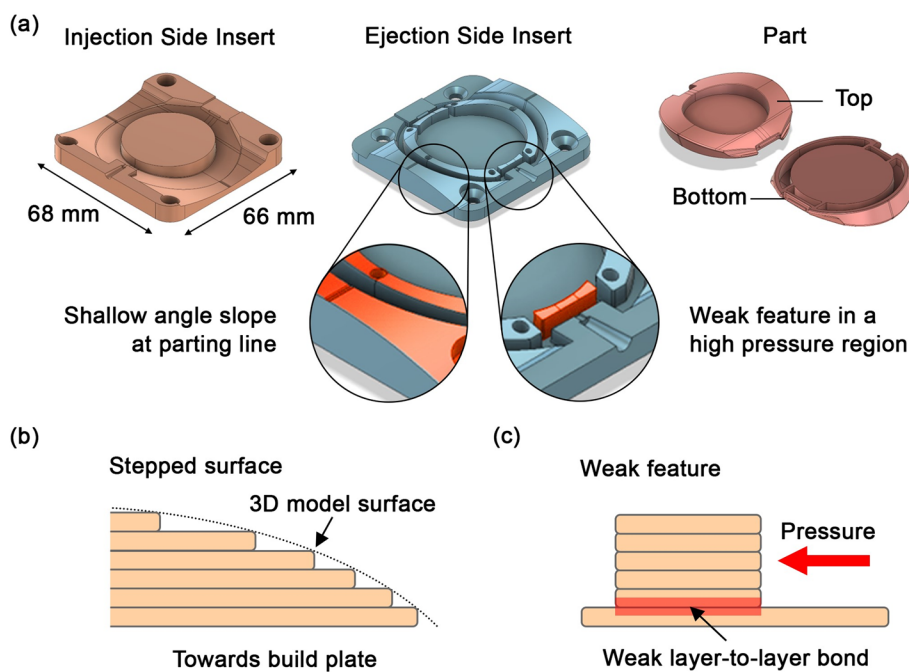
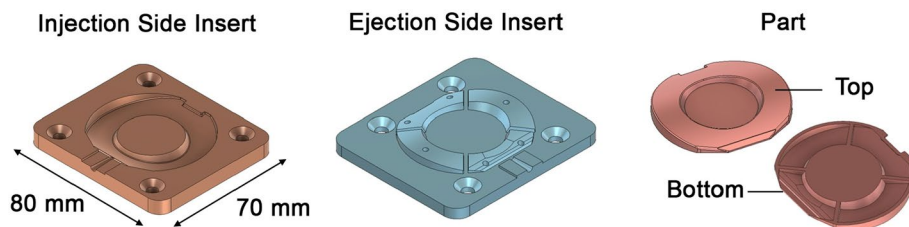


**Fig. 3** Case study 2 inserts and part



the 3D printer can resolve the surface curves, as shown in Fig. 2b. The issue may be remedied by using 5 axis or non-planar 3D printing process which in practice can follow the ideal 3D model surface. Future studies could employ one or both technologies to improve the insert geometry fidelity. Another relevant issue is poor z strength i.e., interlayer bond strength which can lead to premature part failure. Case study 1 has a good example for such a feature, highlighted in the right, magnified region of Fig. 2a. As illustrated in Fig. 2c, the pressure generated by the molten polymer starting to fill the insert will leverage on the weak layer-to-layer bond, possibly leading to breakage [24]. The aforementioned issues led to drafting of another case study with a simpler geometry, better suited to MEX processes.

The second case study, as shown in Fig. 3, has a flat contact surface instead of the shallow curved surface that existed in case study 1. The change is illustrated further in Fig. 4 where both case studies are compared side by side. The part itself, nevertheless, still has a shallow curved surface which will be 3D printed as stepped terraces. A flat contact surface should improve the watertightness of the mold which in turn would improve the quality of the parts produced. The

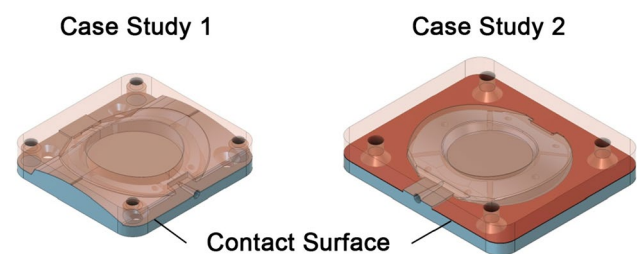


**Fig. 4** Contact surface of case study 1 and 2

part ribbing was also altered to remove the occurrence of weak features, especially in front of the injection point [24]. Finally, the insert was also widened to increase the distance between the fasteners holding the insert to the mold. Both inserts were FGF 3D printed and subsequently tested using injection molding.

## 2.2 Material, equipment and insert production

The inserts were 3D printed out of ULTEM 9085 in granulate form, supplied by Ensinger Plastics (Germany). The

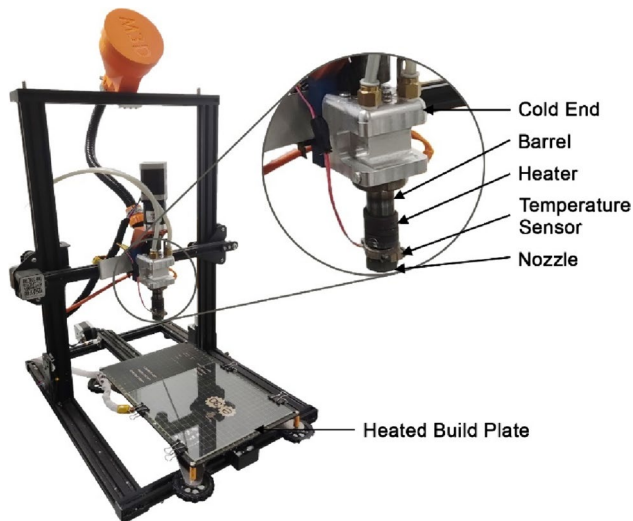


Fig. 5 FGF setup with magnified granulate extruder

Table 1 Screw geometric dimensions

	Length (mm)	Turns	Helix angle (°)	Depth (mm)
Feeding section	38.25	2.73	17.66	4.0
Compression section	38.25	–	–	–
Metering section	8.5	0.45	22.36	1.5

granules were dried at 140 °C for 4 h prior to 3D printing. An in house developed FGF system, shown in Fig. 5, was used to 3D print the inserts. The system used a 14 mm diameter extrusion screw with variable channel depth and helix angle as listed in Table 1. The extruder was mounted on a CR-10s by Creality (China), as done by Curmi and Rochman [25, 26], using an open chamber configuration. A calibration procedure was undergone a priori to ensure a consistent extrusion rate. Prusa Slicer by Prusa Research (Prague, Czech Republic) was used to slice the 3D models and generate the GCODE to drive the 3D printer.

The inserts were 3D printed flat on a high temperature heated build plate (E3D, United Kingdom), as shown in Fig. 6. The borosilicate glass build plate was cleaned using acetone and heated to 200 °C before each insert was 3D printed. The insert was 3D printed in series i.e., from start to finish before moving on to the next insert. This method ensured the best repeatability for insert production. Two insert pairs were produced per case study as the mold itself has two insert cavities.

The most pertinent process parameters used for 3D printing are listed in Table 2. The nozzle and build plate temperature were selected by following the data provided

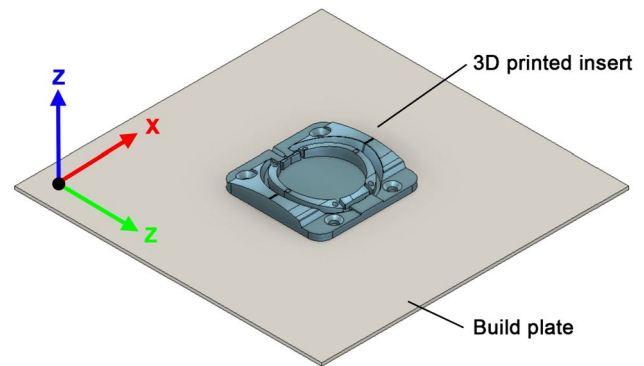


Fig. 6 Insert orientation used for 3D printing

Table 2 FGF 3D printing process parameters

Parameter	Value
Nozzle temperature	310 °C
Build plate temperature	200 °C
Speed	30 mm/s
Infill type	Gyroid
Infill percentage	20%
Perimeter count	4
Number of top layers	8
Number of bottom layers	5
Layer height	0.2 mm
Nozzle size	0.4 mm

by Sabic technical datasheet [21]. The printing speed was set to 30 mm/s to improve the extruder positional accuracy. At this speed, the corners were well-defined and calibration cubes were found to 3D print accurately. The infill was set to 20% gyroid to minimize production times with four outer perimeter, eight top layers and five bottom layers [27]. These settings are commonly used to obtain high, overall, printing speeds while still maintaining good surface quality and strength. The layer height was set to 0.2 mm which is half of the nozzle diameter of 0.4 mm, to further minimize production time.

A dynamic mechanical analysis (DMA) using a Mettler Toledo (USA) DMA 1 in a 3-point bending mode was conducted on parallel and perpendicular FGF 3D printed specimens, as shown in Fig. 7. The 30 × 5 × 2.5 mm specimens were heated from 25 to 150 °C, at 10 μm amplitude at a frequency of 1 Hz, with a 1 N preload, while recording the storage modulus ( $M'$ ).

### 2.3 Insert and part dimensional analysis

Inserts and subsequent parts produced by the injection molding process had some level of unwanted warpage and

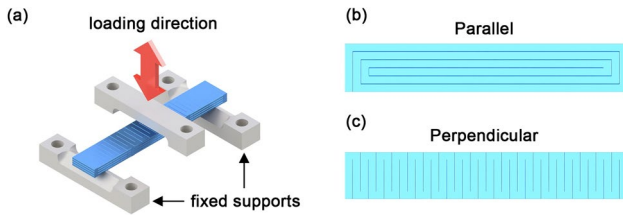


**Fig. 7** 3-point bending DMA setup (a) with parallel (b) and perpendicular (c) orientation

geometric inaccuracy imparted to them. The dimensional accuracy of both inserts and parts produced was analyzed by optical profilometry using a Bruker Alicona G5 Infinite Focus (Austria) measurement system. In each case, the surface of a representative specimen was 3D scanned and then the resulting data was compared with the original 3D surface model, as illustrated in Fig. 8. Cloud Compare open-source software [28] was used to carry out the comparison. The ideal and surface models were 3D registered and the difference between both models was calculated using the mesh to cloud program available in Cloud Compare.

### 2.4 Simulation and experimental injection molding

The injection molding process was simulated using Autodesk Moldflow Insight 2023 with a standard fill and pack strategy. The simulation predicted the warpage of the molded part after its ejection/demolding from the mold inserts. The simulation results were then compared with the optical profilometry results of the produced parts. The mold material properties used are listed in Table 3. The cooling time was set to 300 s with an isothermal mold temperature of 25 °C. Moldflow Insight does not have built-in additive manufacturing functionality for molds nor does it have a dedicated library for AM produced inserts. The values selected were the closest available approximation to the expected properties and attributes of 3D printed ULTEM 9085. This is a limitation of the study whereby future works may focus further on the simulation aspect.

The inserts and mold were mounted on a BOY 22E injection molding machine with a 22 mm diameter screw and maximum clamping force of 220 kN. The mold temperature was controlled using a Singer temperature control unit and

**Table 3** Mold material properties used for simulation [21, 29, 30]

Mold	Value
Density [21]	1.34 g/cm <sup>3</sup>
Specific heat [29]	50 J/kg K
Thermal conductivity [30]	0.25 W/m K
Coefficient of thermal expansion [21]	6.5e-5 1/K
Elastic modulus [21]	3000 MPa
Poisson ratio [21]	0.4

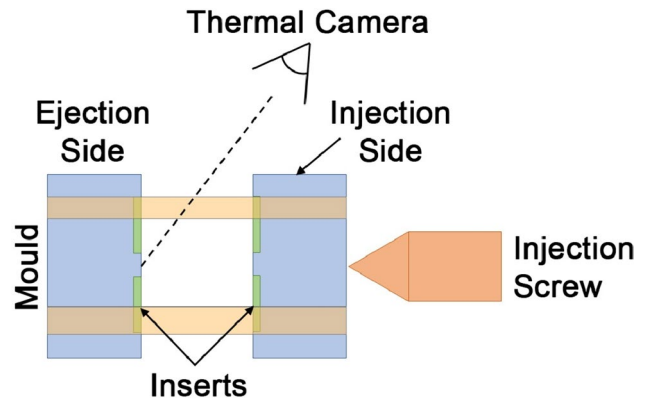
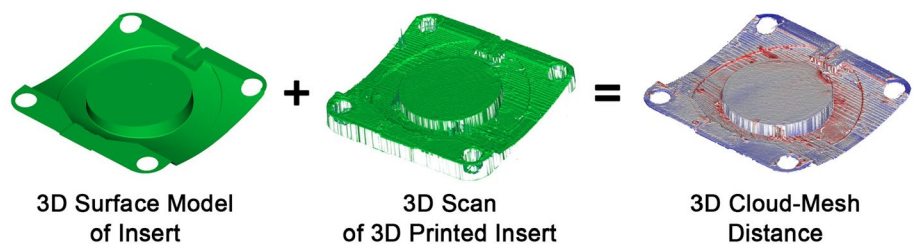


**Fig. 9** Schematic diagram of thermal camera location with injection molding setup

was kept at 25 °C to allow for faster mold cooling. The parts were injection molded using MOPLAN HP501L polypropylene (PP) by LyondellBasel (Netherlands) [31] with a barrel temperature set to 190 °C. Since the inserts were printed using a low thermal conductive polymer, a long cooling time of about 265 s was used. The injection molding cycles were repeated until the insert failed.

The injection molding process was recorded using an E95 thermal camera by Teledyne FLIR LLC (USA) with setup shown in Fig. 9. The emissivity ( $\epsilon$ ) of ULTEM 9085 was determined to be 0.85 by heating a specimen in a furnace to 100 °C and then measuring the surface temperature using an E95 thermal camera. Temperature measurement was started when the mold began to open after the set cooling time was reached. The thermal camera recorded the mold insert's temperature of the ejection side as they cooled. FLIR Research

**Fig. 8** 3D ideal versus scan comparison method



IR Max was used to process the recorded video and extract the cooling rate at different locations on the inserts.

### 3 Results and discussion

#### 3.1 Insert production and evaluation

Production of inserts using an FGF system follows a similar process to filament-based systems, with the key difference lying in the raw material. ULTEM 9085 as granules offer identical physical properties to its filament counterpart (unless modified), but at a significantly lower cost. ULTEM

9085 granules costs around 140 €/kg, nearly half the price of their filament counterpart (260 €/kg) [32, 33]. This positions ULTEM9085 granules similarly to the standard gray resin provided by Formlabs (130 €/kg) and even to the high-temperature version (200 €/kg), which are for a Vat polymerization process and would be more suitable for this application [34, 35]. Therefore, FGF using granules offers a cost-effective alternative since the cost of ULTEM 9085 is similar to the cost of the basic resins' materials used for the Vat polymerization process. However, a trade-off exists between the cost and inserts properties. While the Vat polymerization generally boasts a smoother surface finish, FGF excels in material strength and, consequently, inserts' longevity. Production time compared to Vat polymerization might be slower, but the time difference is often negligible.

The inserts produced via FGF were of good apparent quality as shown in Fig. 10. As expected, the shallow curved surfaces were printed as terraced sections. The terracing effect could have been mitigated by using a smaller layer height or a completely different AM processes such as vat polymerization which could achieve even smaller layer heights, as shown by Vella et al. [11].

The results of the more detailed optical profilometry inspection of case study 1 inserts are shown in Fig. 11a. All inserts were printed with a dimensional difference smaller than  $\pm 0.5$  mm. These values were determined using Chebyshev's theorem using a 95% range. This range is intended to remove any trivial strands and artifacts which in practice are easy to remove and are not relevant for the analysis. The range between  $\pm 0.5$  and  $\pm 1$  mm was grayed out as only strands and other easily removable artifacts are present in this range.

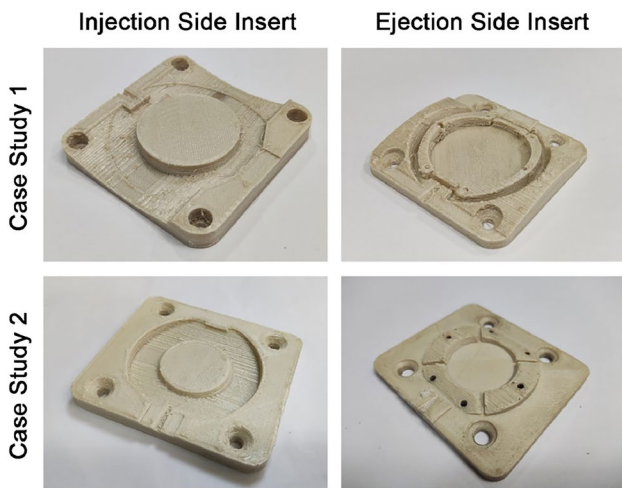
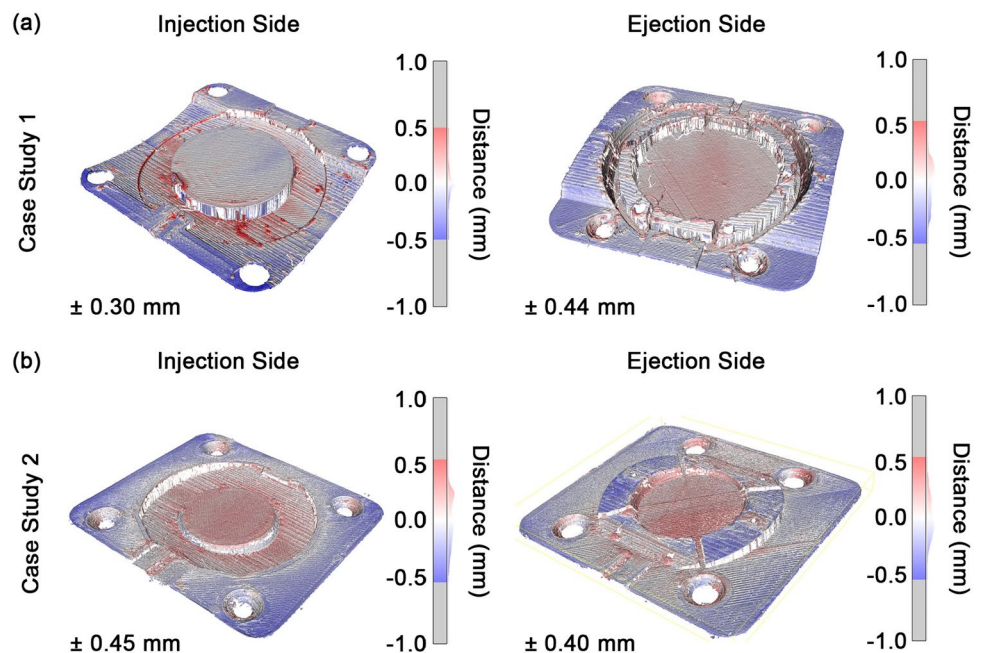


Fig. 10 FGF 3D printed inserts

Fig. 11 Dimensional fidelity analysis for case study 1 and 2 with 95% displacement value range using Chebyshev's theorem



All results showed in Fig. 11 suggest that the inserts were convexly warped i.e., the internal region is higher than the external region of the inserts. This dimensional study also confirmed that the terraced and shallow curved surfaces were 3D printed with the outer edge following the 3D model surface, as illustrated in Fig. 2b. Therefore, this is a clear indication that case study 1 is not watertight. Similarly, case study 2 is also not watertight since the flat contact/clamping surface area has micro paths which leave gaps in the order of  $10^{-1}$  mm, as shown in the representative profilometry results in Fig. 12. Such gaps are sufficient to leak polymer melt during injection. This is supported by the work of Menges et al. which defined a recommended vent thickness of 0.015 mm to ensure no leakages for low viscosity materials [36]. It should be noted that during actual injection molding, the inserts were compressed on each other which may cause a certain amount of crushing. Therefore, once the inserts are compressed, the effective gap between the faces might be of a smaller order than as discussed.

Apart from the warpage and general lack of watertightness, the 3D printed inserts had areas of over-extrusion and blobbing. Such regions are marked with sharp reds in Fig. 11, with the most prominent example being the injection side insert of the case study 1. These artifacts are easily removable by hand but leave a blemish upon removal. A high retraction or screw reversing value of the FGF system may decrease the occurrence of such defects given that they are commonly caused by drooling.

### 3.2 Part production and failure analysis

The case study 1 inserts failed at the first injection molding run. The ejector pins were unable to push out the molded part from the insert. This caused the insert to rip out from the mold as shown in Fig. 13 with the parts still attached. Since the case study 1 inserts had a large surface area with a rough surface finish, the molten polymer could get ingrained within the layer lines. This led to a strong bond between the

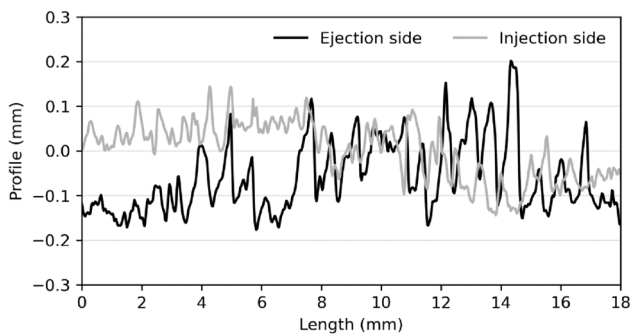


Fig. 12 Representative profile of ejection and injection contact surface obtained by optical profilometry



Fig. 13 Ejection side, case study 1, insert failure at first injection run

molded part and the insert so that the ejector pins failed to demold the molded parts without damaging them and/or the inserts. The large amount of flashes formed, as shown in Fig. 13, was caused by the blockage of the other cavity which led to an overflow of material.

In contrast to the case study 1 inserts, the case study 2 inserts did not fail. They were used for 18 molding cycles of which the first 5 cycles were only partially filled, as listed in Table 4. These first shots were underfilled to avoid premature insert failure. The shot volume had to be increased beyond the theoretical target part volume, to be able to completely fill the cavity and account for the flashing. This flash formation was attributed to the poor water tightness of the inserts as described previously. The extra material also filled the thin space between the insert and metal cavity plate, which in turn partially stuck the parts to the mold, as shown in Fig. 14. It was also noted that during injection molding,

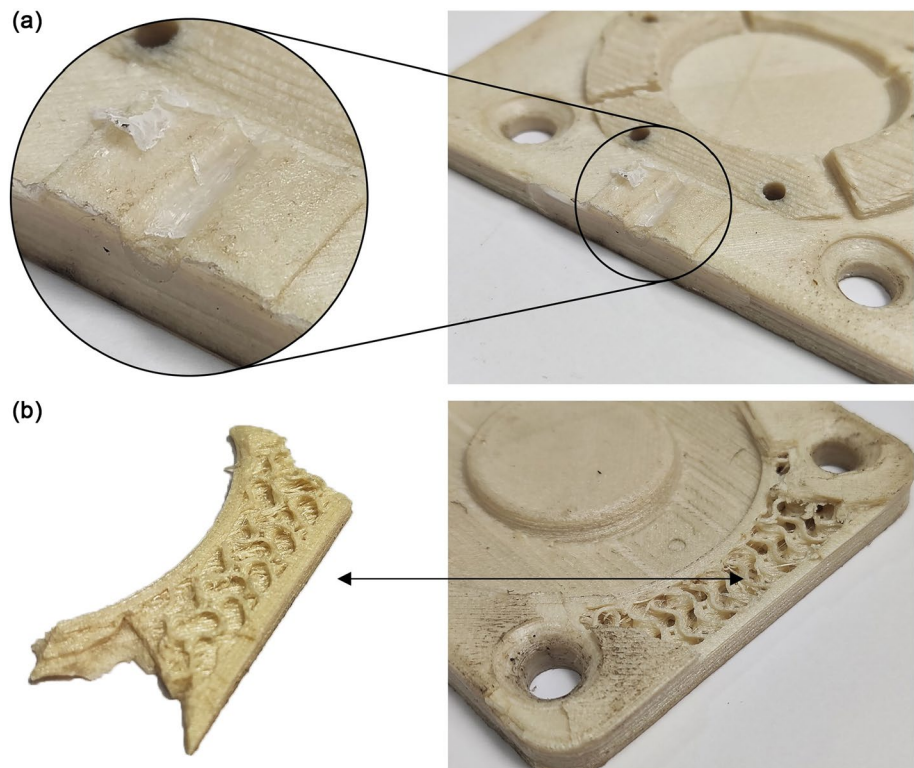
Table 4 Case study 2 injection molding detailed run description

Trial	Shot volume (ccm)	Fill rate (estimate)	Damage to insert
1	10	Partial	None
2	10	Partial	None
3	11.1	Partial	Material removal at outer edge
4	12.4	Partial	Material removal at outer edge
5	14.5	Partial	Material removal at outer edge
6	15.5	Filled	Material removal at outer edge
7	15.5	Filled	Material removal at outer edge
8	15.5	Filled	None
⋮	⋮	⋮	⋮
18	15.5	Filled	None



**Fig. 14** Parts of case study 2 as produced during injection molding. The parts were stuck to the sides of the inserts due to flash, even after ejection

**Fig. 15** Failure modes of case study 2 inserts



there was a slow but progressive removal of material from weak points in the ULTEM 9085 inserts, such as at corners or sharp edges. This gradually decreased the structural integrity of the inserts and led to failure.

Two types of failures were noted. The first one involves the molten PP being stuck in the features of the inserts, as shown in Fig. 15a. This occurrence did not create any direct part defects or any instabilities in the molding process. The second type of failure is more relevant as it led to the insert failure. In this case, one of the two injection side inserts failed through interlaminar cracking, as shown in Fig. 15b. Failure was caused by the action of pulling the part out of the injection side insert. This motion created a perpendicular stress on the insert which acts on the weakest direction of FGF 3D printed parts i.e., the inter-layer bond [2, 3].

Another contributing factor to the inserts' failure is temperature. The thermal images of the mold are shown in Fig. 16 with detailed cooling curves illustrated in Fig. 17. After mold opening, the maximum insert/part temperature was around 130 °C which is lower than the heat deflection temperature (HDT) as listed in the material datasheet [21]. Nonetheless, the barrel temperature was set to 190 °C, and therefore, during the initial stages of injection, the inserts could be hotter than the HDT tested at 1.82 MPa and 153 °C. This could partly be the cause behind the gradual removal of material from the insert edges after multiple runs in contact with the hot melt. The thermal imaging also confirmed that when injecting PP in ULTEM 9085 inserts, a long cooling time with an open mold of about 170 s is necessary to get the



**Fig. 16** Thermal images of injection molding cycle

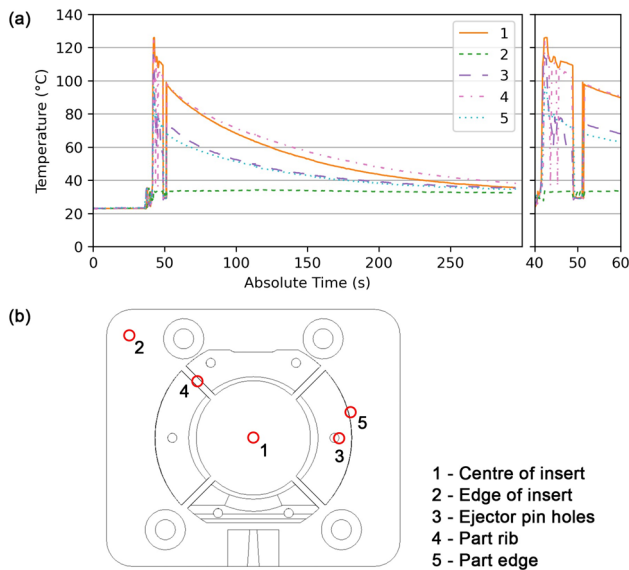
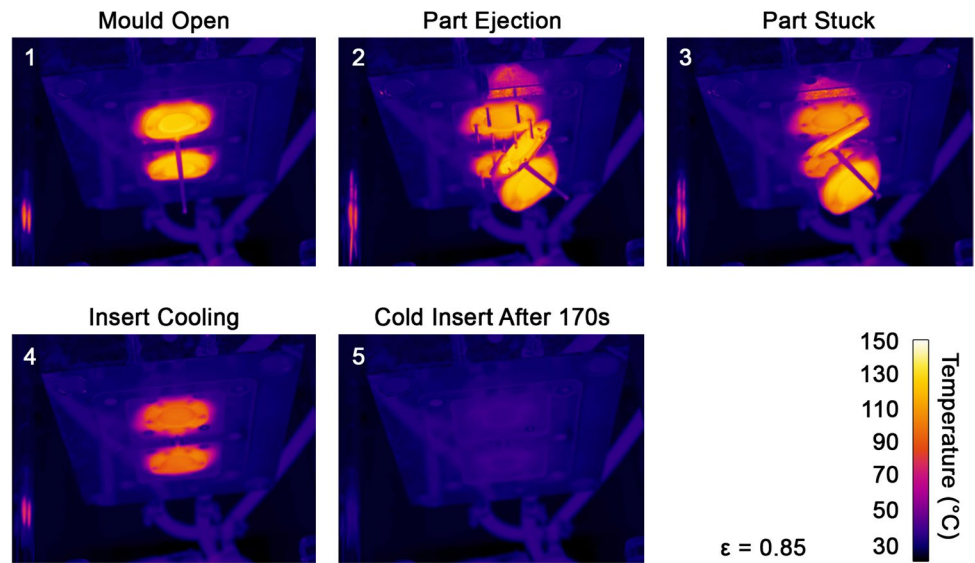


**Fig. 17** Cooling curves (a) of discrete points on the ejection side insert (b)

mold back to room temperature. Without this extra cooling process, the heat accumulation in the inserts could lead to an accelerated degradation.

The detailed cooling curves shown in Fig. 17 demonstrate the change in temperature along the ejection side insert. It should be noted that the disturbance seen around the 50 s mark was caused during the removal of the stuck part. The insert heating and cooling process seemed inhomogeneous being highest at the center (1) of the insert and at the rib (4) sections. The part regions adjacent to the ejector pins (3) and insert’s edge (5) cooled at a similar rate. Any simulation carried out in future work should,

therefore, account for the cooling effect of ejector pins. The outer region of the insert was completely cool with barely any change registered during the whole cooling cycle. At mold opening, the difference in temperature between the center of the mold and outer regions was about 80 °C. Such a large temperature difference may lead to the generation of internal stresses and insert warpage caused by the thermally expanded center of the insert. In this case, ULTEM 9085 is a rather ductile material [21] and can absorb the extra load caused by the constrained, localized thermal expansion. A brittle material could fail prematurely because of thermal expansion. Vat polymerization resins tend to be brittle, and therefore, for RTIM application, modified grades for increased toughness should be used.

The highest temperature recorded by thermal imaging was less than 130 °C. In contrast, the DMA results shown in Fig. 18 indicated that FGF 3D printed ULTEM 9085 maintained a high  $M'$  until about 140 °C. This compares favorably with vat polymerization material, such as Rigid 10k and HighTemp by Formlabs. The DMA conducted by Moritz et al. [6] demonstrated that while these materials tend to have a higher  $M'$  at room temperature, it is not maintained over the whole molding temperature range. By 100 °C, the resins would have softened significantly whereas the 3D printed ULTEM 9085 maintained similar  $M'$  until about 140 °C. The DMA results also demonstrate that the perpendicularly printed specimens, representing the strand-to-strand bond, had half the storage modulus of parallelly printed specimens. This further confirms the weak interlayer bond created by the respective printing parameters and setup used in this study, leading to the failure shown in Fig. 15b. Future studies may use a heated chamber coupled with a

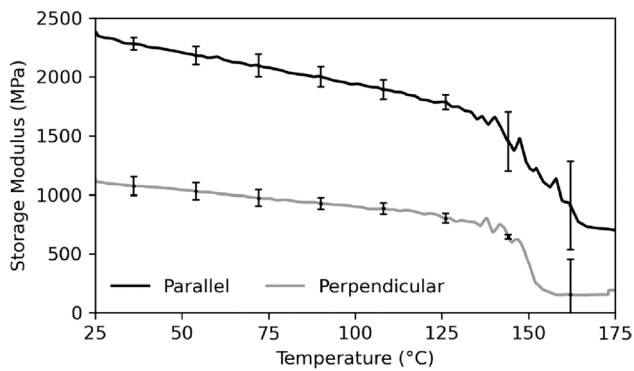


**Fig. 18** DMA of parallelly and perpendicularly 3D printed ULTEM 9085 ( $n=3$ )

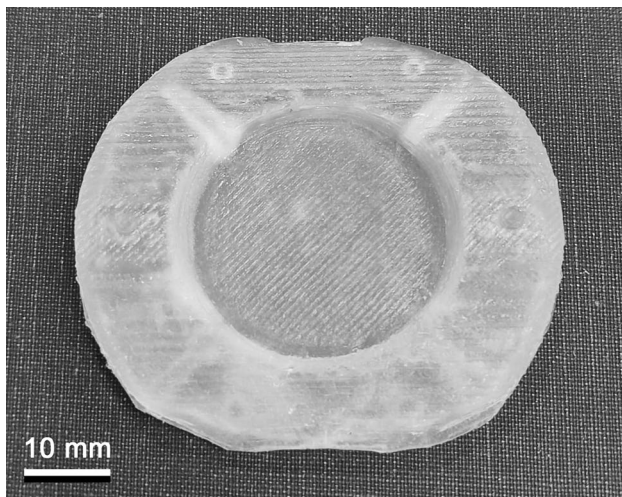


**Fig. 19** Representative injection molded part with flash removed

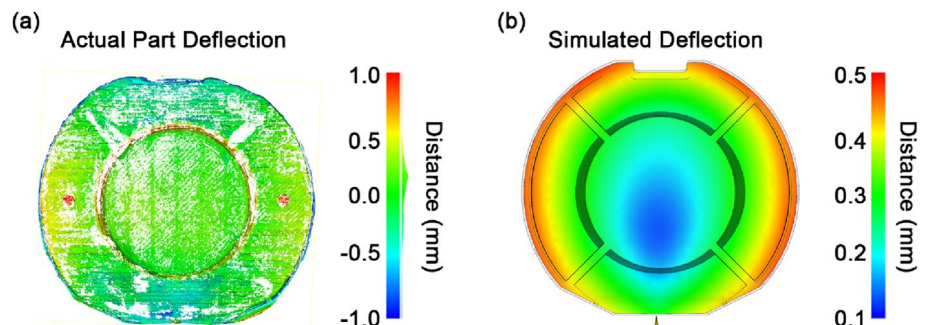
higher extrusion temperature, to improve the layer-to-layer bond strength and thus improve insert longevity.

### 3.3 Part quality

A molded part is shown in Fig. 19, with the extra flash removed as a representative molding result. Most of the PP molded part is slightly transparent which indicates that a large share of PP part was amorphous. Transparency decreased at the ribbed sections of the parts and at the injection point, creating opaque regions. Such regions are caused by hot spots created by the poor thermal conductivity of ULTEM 9085, which limited heat dissipation. These hotter regions led to a prolonged period of high temperature which allowed for crystallization of the PP, indicated by the opacity at those hot spots only. Apart from changes in color, crystallization also changed mechanical properties and density. In the latter case, the result is a densification of the PP leading to a decrease in volume at the crystallized region, creating differential shrinkage thus warping the part. In general, shrinkage at the crystallized area pulls in the surrounding region causing a bending effect along with localized stresses in the part. Any dimensional tolerances required of the part are, therefore, compromised unless crystallization is accounted for in the design [37]. Furthermore, the mechanical behavior of the part becomes a complex mix of amorphous and crystalline PP properties further complicated by localized, internal stresses. In this manner, the part is inhomogeneous which is undesirable in most applications. Localized hot spots may also lead to other undesirable features such as sink marks which are more prevalent for thicker parts [38]. In the end, the product would not have the desired properties or the apparent quality for the final application.

All parts produced had a rough surface with a clear imprint of the FGF 3D printed insert strand lines and terraced shallow curves. Optical profilometry results, shown in Fig. 20a, demonstrated that the parts warped with a deviation from the ideal geometry of  $\pm 0.60$  mm for 95% of the top surface. The simulated deflection is shown in Fig. 20b. There is a significant discrepancy between the two results as the simulation results grossly

**Fig. 20** Part warpage as observed using optical profilometry (a) and as predicted by simulation (b)



underestimating the deflection to about  $\pm 0.2$  mm. Furthermore, as seen from top view of actual part deflection in Fig. 20a, the side portions of the part are deflected outwards as opposed to the top and bottom portions. Therefore, the simulated deflection shape did not agree with the actual part deflection.

The discrepancy between these two results may be caused by two aspects. The first concerns the ejection process. Upon mold opening and ejection, the part temperature was the same as that of the insert, reaching 130 °C, as shown in Fig. 16. At that temperature, PP is beyond its softening temperature [31] and therefore, the ejection process was conducted on a soft part, with poor shape retention. This effect is expected to increase the part's warpage, beyond what was directly caused by differential shrinkage. The second is related to insert temperature and the discrepancy in temperature between different points on the insert, as observed by the thermal imaging results of Fig. 17. The Moldflow simulation with pack and fill strategy may not be optimized for such slow heat transfer and may assume that the insert is at a stable 25 °C, leading to the lower deflection. Even if the simulation had correctly calculated the cooling rate, the ejector pin issue would have nullified the warpage results anyway as the simulation cannot take that kind of action into account. Therefore, due to the high, undesired but unavoidable flashing of the parts and the related anchorage of part with insert, simulating warpage is not deemed feasible for FGF printed inserts.

## 4 Conclusion

This study demonstrated for the first time that rapid tooling of injection mold inserts manufactured using ULTEM 9085 with an open chamber FGF system are amenable to produce small quantities of molded parts intended for prototyping purposes. In one case, a total of 28 parts were produced until the insert failed. The Moldflow simulation undervalued the amount of part deflection and even the general warpage shape. This was attributed to the slow cooling speed of the inserts and the action of the ejector pins pushing on the still hot, molded parts. The part geometry complexity was found to affect the viability of the rapid tooling process. Simpler geometries with a lower amount of anchorage points that are unintentionally created by the layered nature of MEX 3D printing system are better suited for rapid tooling of injection mold inserts. FGF 3D printed inserts are expected to produce parts with flash. A flat surface 3D printed using a 0.4 mm nozzle, will have surface perturbations large enough to allow polymer melt to flow. ULTEM 9085 demonstrated its applicability for RTIM as it maintained a high storage modulus up to 140 °C.

**Acknowledgements** The authors thank all partners involved in the MALT3D project for their continuous support.

**Funding** Open Access funding provided by the University of Malta. This work was part of the MALT3D research project funded by the Malta Council for Science and Technology through the FUSION: R&I Technology Development Programme (R&I-2018-009T).

**Data availability** Data will be made available on request.

## Declarations

**Conflict of interest** The authors declare that there is no conflict of interest.

**Open Access** This article is licensed under a Creative Commons Attribution 4.0 International License, which permits use, sharing, adaptation, distribution and reproduction in any medium or format, as long as you give appropriate credit to the original author(s) and the source, provide a link to the Creative Commons licence, and indicate if changes were made. The images or other third party material in this article are included in the article's Creative Commons licence, unless indicated otherwise in a credit line to the material. If material is not included in the article's Creative Commons licence and your intended use is not permitted by statutory regulation or exceeds the permitted use, you will need to obtain permission directly from the copyright holder. To view a copy of this licence, visit <http://creativecommons.org/licenses/by/4.0/>.

## References

- Gibson I (2005) Rapid prototyping: a tool for product development. *Comput Aided Des Appl* 2:785–793. <https://doi.org/10.1080/16864360.2005.10738342>
- Shelton TE, Willburn ZA, Hartsfield CR et al (2020) Effects of thermal process parameters on mechanical interlayer strength for additively manufactured Ultem 9085. *Polym Test* 81:106255. <https://doi.org/10.1016/j.polymertesting.2019.106255>
- Zaldivar RJ, Witkin DB, McLouth T et al (2017) Influence of processing and orientation print effects on the mechanical and thermal behavior of 3D-Printed ULTEM® 9085 Material. *Addit Manuf* 13:71–80. <https://doi.org/10.1016/j.addma.2016.11.007>
- Davoudinejad A, Khosravani MR, Pedersen DB, Tosello G (2020) Influence of thermal ageing on the fracture and lifetime of additively manufactured mold inserts. *Eng Fail Anal* 115:104694. <https://doi.org/10.1016/j.engfailanal.2020.104694>
- Davoudinejad A, Bayat M, Pedersen DB et al (2019) Experimental investigation and thermo-mechanical modelling for tool life evaluation of photopolymer additively manufactured mould inserts in different injection moulding conditions. *Int J Adv Manuf Technol* 102:403–420. <https://doi.org/10.1007/s00170-018-3163-7>
- Moritz VF, Bezerra GSN, Hopkins Jnr M et al (2022) Heat dissipation plays critical role for longevity of polymer-based 3D-printed inserts for plastics injection moulding. *JMMP* 6:117. <https://doi.org/10.3390/jmmp6050117>
- Mischkot M, Davoudinejad A, Charalambis A et al (2017) Dimensional accuracy of Acrylonitrile Butadiene Styrene injection molded parts produced in a pilot production with an additively manufactured insert
- Dizon JRC, Valino AD, Souza LR et al (2020) 3D printed injection molds using various 3D printing technologies. *MSF* 1005:150–156. <https://doi.org/10.4028/www.scientific.net/MSF.1005.150>

9. Walsh E, Ter Horst JH, Markl D (2021) Development of 3D printed rapid tooling for micro-injection moulding. *Chem Eng Sci* 235:116498. <https://doi.org/10.1016/j.ces.2021.116498>
10. Dempsey D, McDonald S, Masato D, Barry C (2020) Characterization of stereolithography printed soft tooling for micro injection molding. *Micromachines* 11:819. <https://doi.org/10.3390/mi11090819>
11. Vella A, Arif R, Pierre V (2023) Rapid tooling development for low volume injection molding of cosmetic compacts. *Mater Res Forum*. <https://doi.org/10.21741/9781644902479-23>
12. Rodzeń K, Harkin-Jones E, Wegrzyn M et al (2021) Improvement of the layer-layer adhesion in FFF 3D printed PEEK/carbon fibre composites. *Compos A Appl Sci Manuf* 149:106532. <https://doi.org/10.1016/j.compositesa.2021.106532>
13. Altaf K, Rani AMA, Ahmad F, Ahmad J (2018) Enhanced polymer rapid tooling for metal injection moulding process. In: *PRO-AM conference papers*
14. Altaf K, Qayyum J, Rani A et al (2018) Performance analysis of enhanced 3D printed polymer molds for metal injection molding process. *Metals* 8:433. <https://doi.org/10.3390/met8060433>
15. Boros R, Kannan Rajamani P, Kovacs JG (2019) Combination of 3D printing and injection molding: overmolding and overprinting. *Express Polym Lett* 13:889–897. <https://doi.org/10.3144/expresspolymlett.2019.77>
16. Gohn AM, Brown D, Mendis G et al (2022) Mold inserts for injection molding prototype applications fabricated via material extrusion additive manufacturing. *Addit Manuf* 51:102595. <https://doi.org/10.1016/j.addma.2022.102595>
17. Zink B, Kovács NK, Kovács JG (2019) Thermal analysis based method development for novel rapid tooling applications. *Int Commun Heat Mass Transf* 108:104297. <https://doi.org/10.1016/j.icheatmasstransfer.2019.104297>
18. Tomori T, Melkote S, Kotnis M (2004) Injection mold performance of machined ceramic filled epoxy tooling boards. *J Mater Process Technol* 145:126–133. [https://doi.org/10.1016/S0924-0136\(03\)00881-1](https://doi.org/10.1016/S0924-0136(03)00881-1)
19. Sá Ribeiro A, Hopkinson N, Henrique Ahrens C (2004) Thermal effects on stereolithography tools during injection moulding. *Rapid Prototyp J* 10:176–180. <https://doi.org/10.1108/13552540410538996>
20. Zhang Y, Moon SK (2021) The effect of annealing on additive manufactured ULTEM™ 9085 mechanical properties. *Materials* 14:2907. <https://doi.org/10.3390/ma14112907>
21. Sabic ULTEM™ RESIN 9085 global technical data sheet
22. Farioli D, Strano M, Vangosa FB et al (2021) Rapid tooling for injection molding inserts. *ESAFORM 2021*. <https://doi.org/10.25518/esaform21.4186>
23. Roozenburg NFM, Eekels J (1995) *Product design: fundamentals and methods*. Wiley, Chichester
24. Bagalkot A, Pons D, Symons D, Clucas D (2021) Analysis of raised feature failures on 3D printed injection moulds. *Polymers* 13:1541. <https://doi.org/10.3390/polym13101541>
25. Curmi A, Rochman A (2022) From theory to practice: development and calibration of micro pellet extruder for additive manufacturing. *Key Eng Mater* 926:34–45. <https://doi.org/10.4028/p-b22a9a>
26. Curmi A, Rochman A (2023) Miniaturized fused granulate fabrication of polyether ether ketone (PEEK). *Prog Addit Manuf*. <https://doi.org/10.1007/s40964-023-00518-4>
27. Ćwikła G, Grabowik C, Kalinowski K et al (2017) The influence of printing parameters on selected mechanical properties of FDM/FFF 3D-printed parts. *IOP Conf Ser Mater Sci Eng* 227:012033. <https://doi.org/10.1088/1757-899X/227/1/012033>
28. (2023) *CloudCompare* (version 2.13) [GPL software]
29. Li H, Taylor G, Bheemreddy V et al (2015) Modeling and characterization of fused deposition modeling tooling for vacuum assisted resin transfer molding process. *Addit Manuf* 7:64–72. <https://doi.org/10.1016/j.addma.2015.02.003>
30. *Manufacture of Fused Deposition Modeling Joints using ULTEM 9085*
31. *LyondellBasell (2023) Moplen HP501L technical data sheet*
32. *PEI 9085 Pellets | Filament2Print*. <https://filament2print.com/gb/pellets-and-coloring/1308-pei-9085-pellets.html>. Accessed 23 Jan 2024
33. *PEI Ultem 9085 Filament*. In: *3D4Makers.com | 3D Printing Filament*. <https://www.3d4makers.com/products/pei-ultem-9085-filament>. Accessed 23 Jan 2024
34. *Grey Resin*. In: *Formlabs*. <https://formlabs.com/eu/store/materials/grey-resin/>. Accessed 23 Jan 2024
35. *High Temp Resin*. In: *Formlabs*. <https://formlabs.com/eu/store/materials/high-temp-resin/>. Accessed 23 Jan 2024
36. Kazmer DO (2016) Venting. In: *Injection mold design engineering*. Carl Hanser Verlag GmbH & Co. KG, pp 227–242
37. Lerma Valero JR (2020) Chapter 2—Thermodynamic behavior of plastics: PVT graphs. In: Lerma Valero JR (ed) *Plastics injection molding*. Hanser, pp 25–34
38. Lerma Valero JR (2020) Chapter 25—Defects in injection molded parts. In: Lerma Valero JR (ed) *Plastics injection molding*. Hanser, pp 328–344

**Publisher's Note** Springer Nature remains neutral with regard to jurisdictional claims in published maps and institutional affiliations.